Analysis of the resonantly photopumped Na-Ne x-ray-laser scheme

Joseph Nilsen and Elaine Chandler
Lawrence Livermore National Laboratory, Livermore, California 94550
(Received 17 January 1991; revised manuscript received 14 June 1991)

This paper analyzes the resonantly photopumped Na-Ne x-ray-laser scheme that has been studied experimentally on Z pinches for the last five years. By modeling as an x-ray source the Na Z-pinch output obtained on the Saturn generator experiments at Sandia National Laboratories, the time-dependent properties of the Ne lasant are studied. Our model yields a maximum gain, approximately 0.2 cm^{-1}, with a full width at half maximum duration of 18.5 ns, on the $4f \rightarrow 3d$ transition at 231 Å under the conditions of the Saturn experiments. We investigate the effects of varying parameters such as the ion density of the Ne lasant and the linewidth of the Na pump line. The impact of radiation trapping on the gain of the various laser lines is considered in a one-dimensional slab geometry.

PACS number(s): 42.60.By, 32.30.Rj

I. INTRODUCTION

Resonant photopumping was one of the original mechanisms proposed for demonstrating x-ray lasing [1,2]. Over the last 15 years many scientists [3-20] have studied this lasing mechanism, both experimentally and theoretically, in the hope of developing a high-efficiency x-ray laser. However, the resonant photopumping mechanism has not yet been demonstrated in the soft-x-ray region with the possible exception of the recently demonstrated lasing in Ne-like Ti at 326.5 Å [21]. Otherwise, the shortest wavelength at which significant gain has been measured using resonant photopumping is in Be-like C [22] at 2163 Å, far outside the x-ray region.

Over the last five years extensive experimental work has been done on the Na-Ne x-ray-laser scheme by using Z pinches to produce a strong He-α Na line to drive the He-like Ne laser [8-10]. Until recently most experiments had tried to create the Na and Ne plasmas by imploding both the Na and Ne gases in separate Z pinches. With the advent of the more powerful Saturn Z pinch, experiments are being done in which the Ne plasma, placed 2 cm from the center of the Na Z pinch, is heated solely by the x-ray radiation produced by the Na Z pinch. Substantial progress has been made in the Saturn experiments, and recently Na-Ne experiments have been done in which a clear enhancement of the Ne He-γ line relative to the He-β line has been observed [23]. This is a very strong indicator that the predicted photopumping which we describe below is occurring in the Ne plasma on the $n=4 \rightarrow 3$ lines. However no observation of gain has yet been made.

We model the Na-Ne x-ray-laser scheme, which is predicted to lase near 231 Å, based on resonant photopumping of the He-γ line of Ne using radiation from the He-α line of Na. The model calculates the plasma conditions that are produced in a Ne gas illuminated by radiation from a Na Z pinch under the conditions that are believed to be produced at the Saturn facility. The modeling assumes that a cold gas of Ne is driven by the x-ray output of the Na Z pinch; for the Na radiation we use the observed output of the Saturn experiment. In this paper the output of the Na Z pinch is discussed in Sec. II. The atomic model for the Ne plasma is described in Sec. III, and the results of the kinetics calculations on an optically thin Ne plasma are presented in Sec. IV; these results include gain, temperatures, ionization fractions, and other plasma parameters as a function of time. Section V presents the effects of radiation transport as they impact the gain. Section VI summarizes the results presented in this paper.

II. Na Z PINCH

Recent experiments at Sandia National Laboratories on the Na Z pinch at the Saturn facility have measured 10 TW of power in a 35-ns pulse for low-energy x-rays and 200 and 400 GW of power in the He-α and Ly-α lines of Na in a 20-ns pulse [23]. The Na Z pinch consists of an array of eight thin Na wires which, when imploded, produce a plasma 2 cm long by approximately 0.4-cm radius. The Ne gas is contained in a 2-cm long, 0.6-cm square box with windows transparent to x rays. The Ne gas box is aligned with its long axis parallel to the Na Z pinch and with its closest window 2 cm distant from the axis of the Z pinch. We assume that the radiation from the Z pinch isotropically illuminates the inside of an imaginary cylinder which is 2 cm long with a radius of 2 cm. Such a cylinder has a surface area of 50 cm^2. This puts an intensity of 200 GW/cm^2 from the low-energy x rays onto the Ne plasma and an intensity of 4 GW/cm^2 from the He-α line onto the Ne plasma. If one models the low-energy x-rays as being emitted from a blackbody, then the radiation temperatures θ_{BB} can be derived from the power per unit area emitted by the source using

$$I=\frac{(2\pi)^3}{(hc)^3}\frac{\pi^2}{60}c\theta_{BB}^4=1.028\times10^5\theta_{BB}^4(\text{in eV})\frac{\text{W}}{\text{cm}^2}\ . \quad (1)$$

For a 10-TW Na Z pinch with a 4.8-cm^2 emitting area, corresponding to a 0.4-cm radius pinch, one derives a radiation temperature of 67 eV. If one considers a smaller 0.1-cm radius pinch with an emitting area of 1.25 cm^2,

then a 94-eV blackbody is obtained from Eq. (1). We use the diluted 94-eV blackbody; however calculations indicate that the results are insensitive to this choice. For the line radiation it is essential to know the linewidth in order to estimate the radiation temperature of the lines. The He-α and Ly-α lines have been measured with linewidths of 4 eV, but those are believed to be dominated by source and instrument broadening [23]. The actual linewidth is estimated [23,24] to vary from 0.78 to 1.5 eV. These large widths are not surprising given the radial implosion velocities which are as large as 40 cm μs^{-1}. Our nominal calculations use the narrower linewidth as this produces the more optimistic calculation of gain. However, we also show how the gain varies with linewidth (see Fig. 10). For simplicity, the line shape is assumed to be a square pulse and a perfect resonance is assumed between the Na He-α pump line and the Ne He-γ line throughout this paper.

For the temporal pulse shape, a Gaussian with a full width half maximum (FWHM) time duration of 35 ns is used for the blackbody component of the x-ray flux. Superimposed on this is the He-α and Ly-α radiation with a FWHM pulse duration of 20 ns. The line radiation and blackbody radiation are assumed to peak at the same time, 52.5 ns in our calculations. Figure 1 shows the peak x-ray spectral intensity versus photon energy $h\nu$ which is used in the calculations. Figure 2 plots the total x-ray intensity (including lines) versus time which illuminates the Ne plasma. The line radiation represents only 6% of the total intensity and is a small component of Fig. 2. The time history of the He-α line is also shown in Fig. 2 magnified by a factor of 50. It is the low-energy x rays which strip the Ne gas down to He-like Ne; the He-α line radiation then resonantly photopumps ions in the He-like Ne ground state resulting in laser action, as described in the next section.

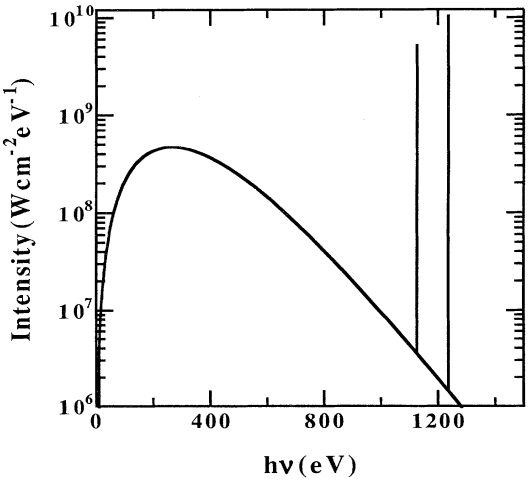

FIG. 1. The x-ray spectral intensity vs photon energy $h\nu$ from the Na Z pinch which illuminates the Ne plasma at the time of peak illumination 52.5 ns. The spectrum includes a diluted 94-eV blackbody spectrum superimposed with Na He-α and Ly-α lines of 0.78-eV width.

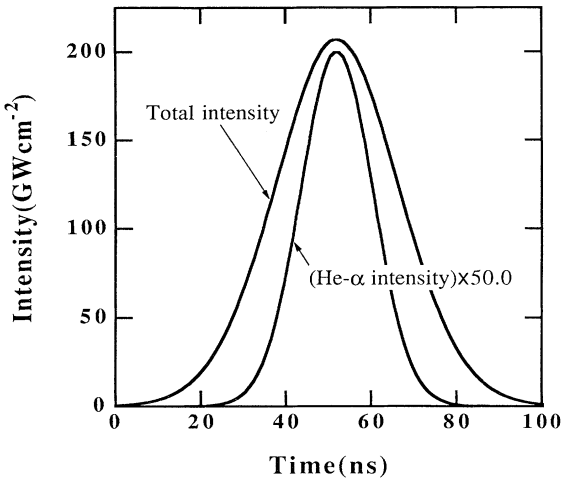

FIG. 2. Intensity vs time for the total x-ray radiation from the Na Z pinch which illuminates the Ne plasma. The 94-eV blackbody component has a 35-ns FWHM Gaussian time history while the weaker He-α component, shown magnified 50 times, is only 20-ns FWHM in duration.

III. BASIC LASER SCHEME AND ATOMIC PHYSICS MODEL

Figure 3 shows the basic lasing scheme which consists of the Na He-α line, $1s2p\ ^1P_1 \rightarrow 1s^2\ ^1S_0$, resonantly photopumping an electron in the ground state of the He-like Ne ion to the $1s4p\ ^1P_1$ level. These two transitions are in almost perfect resonance with the Na He-α line at 11.002 7 Å and the Ne He-γ line at 11.000 3 Å [10,25]. The usual $^{2S+1}L_J$ notation is used to denote the levels.

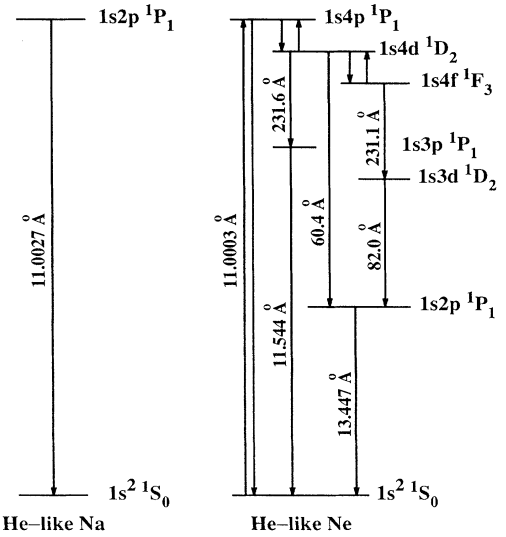

FIG. 3. Na-Ne x-ray laser scheme with the Na He-α line pumping the Ne He-γ transition. Several of the possible laser lines are included. Our calculations show significant gain only on the $4f \rightarrow 3d$ transition at 231 Å.

TABLE I. Laser transitions, wavelengths, and gain for He-like Ne.

Transition	Wavelength (Å)	Gain (cm^{-1}) at $t=52.5$ ns 0D	1D (surface)
$1s4f\ ^1F_3 \rightarrow 1s3d\ ^1D_2$	231.1	0.176	0.157
$1s4d\ ^1D_2 \rightarrow 1s3p\ ^1P_1$	231.6	0.079	0.070
$1s4p\ ^1P_1 \rightarrow 1s3s\ ^1S_0$	222.7	0.021	0.019
$1s4d\ ^1D_2 \rightarrow 1s2p\ ^1P_1$	60.4	0.007	0.003
$1s3d\ ^1D_2 \rightarrow 1s2p\ ^1P_1$	82.0	0.021	−0.016

The $1s4p$ level is partially equilibrated over the other $1s4l$ levels by collisional processes. This establishes a large population in the $1s4f\ ^1F_3$ level, which is the upper laser state for the dominant laser line in the Ne plasma. This state lases to the $1s3d\ ^1D_2$ level, which is the lower laser state. The lower laser state decays to the $1s2p\ ^1P_1$ level, which then decays back to the He-like ground state. Other laser transitions are possible including $4d \rightarrow 3p$, $4p \rightarrow 3s$, $4d \rightarrow 2p$, and $3d \rightarrow 2p$ transitions in the singlet ($S=0$) manifold. These laser transitions, along with their wavelengths, are given in Table I. The weaker laser lines which involve the triplet ($S=1$) manifold are not discussed; however, all the triplet levels are included in the atomic model described below. The wavelengths have been calculated by the authors using the atomic physics code YODA [26], which was also used to construct an atomic model of Ne used in the calculations.

YODA was used to calculate energy levels, oscillator strengths, and collision strengths for the $n=1,2,3$, and 4 states of H-like, He-like, and Li-like Ne. These were combined with simple hydrogenic data for the Rydberg states and the other nearby sequences (Be-like, B-like, and C-like) as well as the photoionization and collisional rates which connect these levels. For He-like Ne, the model consists of 31 detailed levels for levels up to $n=4$ combined with six Rydberg states representing $n=5-10$. Collisions between the He-like singlet and triplet states are included. The $n=4$ manifold of He-like Ne alone consists of 14 levels. The total model consists of 108 levels, 756 lines, 756 collisional excitation rates, 183 collisional ionization rates, and 232 photoionization cross sections. The reverse process to each of these processes is calculated by the XRASER code [27] using detailed balance.

IV. LASER GAIN AND KINETICS

XRASER was used to calculate the time-dependent evolution of the Ne plasma as it was illuminated by the radiation from the Na Z pinch. Using the nominal radiation from the Na Z pinch described in Sec. II, calculations were initially done to determine the optimum density for achieving gain in He-like Ne. These calculations assume that all lines are optically thin. Figure 4 shows the gain of the $4f \rightarrow 3d$ and $3d \rightarrow 2p$ singlet lines at 231 and 82 Å, respectively, versus Ne ion density at the time of peak x-ray illumination, 52.5 ns. The $4f \rightarrow 3d$ line exhibits the strongest gain with its peak at an ion density of 0.8×10^{18} cm^{-3} while the weaker $3d \rightarrow 2p$ line peaks at an ion density of 2.0×10^{18} cm^{-3}. The $4f \rightarrow 3d$ gain decreases as the density increases above 10^{18} cm^{-3} because the collisional equilibration between the $n=4$ and 3 levels of He-like Ne increases the population of $n=3$ at the expense of $n=4$, resulting in higher gain on the $3d \rightarrow 2p$ line. In fact, as the ion density increases above 4.0×10^{18} cm^{-3}, the gain of the $3d \rightarrow 2p$ line overtakes the gain of the $4f \rightarrow 3d$ line; the gain for both lines at these densities is very small. As we show in Section 5, the $3d \rightarrow 2p$ line is very susceptible to radiation trapping effects and will not lase for a laser medium of any reasonable thickness.

In the recent experiments done at the Saturn facility an Ne ion density of 0.4×10^{18} cm^{-3} was used; however it is believed that when the transparent windows on the Ne gas box are heated by the x-ray flux, the windows explode and thereby compress the Ne gas by a factor of 2 or 3 in the region near the surface. Figure 5 plots the H-like, He-like, and Li-like ion fractions versus Ne ion density at the time of peak illumination. The He-like ion fraction is relatively stable over a large range of densities.

Choosing the nearly optimum ion density of 1.0×10^{18} cm^{-3} for gain on the $4f \rightarrow 3d$ line, we then study the time variation of the Ne plasma properties. Figure 6 shows

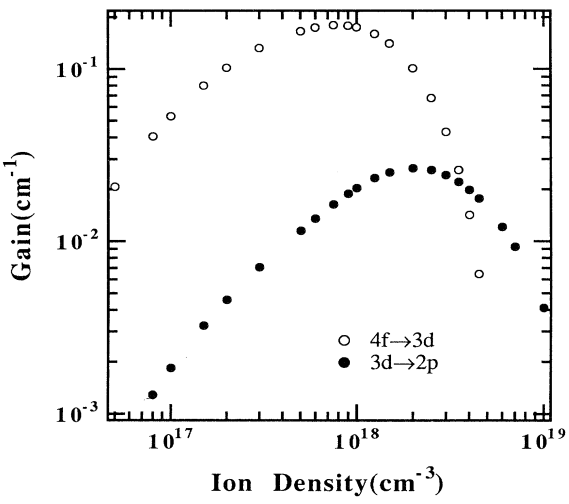

FIG. 4. Gain vs Ne ion density at the time of peak illumination, 52.5 ns, for the $4f \rightarrow 3d$ and $3d \rightarrow 2p$ lasing lines. The $4f \rightarrow 3d$ transition consistently shows the largest gain below 3×10^{18} cm^{-3}. Above this density collisional transitions equilibrate the $n=4$ and 3 levels. These calculations assume an optically thin environment with no radiation trapping effects.

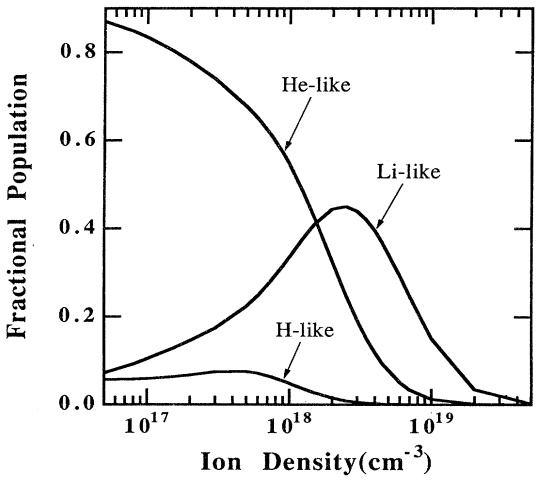

FIG. 5. Fractional ion populations vs Ne ion density at the time of peak illumination 52.5 ns. These populations are relatively insensitive to the ion density in the experimentally accessible region near 10^{18} cm^{-3}.

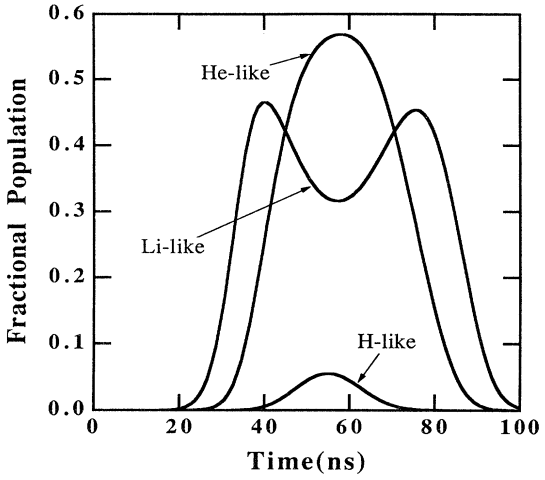

FIG. 7. Fractional ion population vs time for an optically thin Ne model of ion density 10^{18} cm^{-3}. Shortly after the driving pulse peaks at 52.5 ns, Li-like is burnt through and He-like peaks; H-like is produced by the combined action of the Na pump line exciting the Ne $1s$-$4p$ transition followed by ionization of the excited electrons. This process reduces the population of $n=4$ electrons in He-like and lowers the gain.

the electron temperature $\Theta=kT$, in eV, versus time. The electron temperature peaks at 59.5 ns with a value of 26.7 eV. The ion temperature, not shown, is virtually identical with the electron temperature in the calculation. The calculation uses initial ion and electron temperatures of 5 eV for convenience. The time-dependent H-like, He-like, and Li-like ion fractions are shown in Fig. 7. The He-like fraction has a peak value of 56.8% at 58 ns; at the same time there is 31.7% Li-like and 5.2% H-like. The remaining 6.3% is primarily in Be-like. These conditions are excellent for resonantly photopumping the He-like Ne ground state since more than half the Ne population is in the He-like Ne ground state. Our kinetics model indicates that the ionization balance between He-like Ne and Li-like Ne is primarily obtained by balancing the photoionization rate of the $n=2$ electrons in Li-like Ne, a rate of 0.2 ns^{-1}, with the collisional recombination rate of the He-like Ne ground state into the excited Li-like Ne states followed by radiative decay. The small fraction of H-like Ne is mostly due to the resonant photoexcitation of the He-like Ne ground state to the $1s4p$ state followed by photoionization and collisional ionization. Recombination from the H-like Ne ground state plays an insignificant role in populating the He-like Ne $1s4f$ upper laser state.

The gain versus time is presented in Fig. 8 for the three

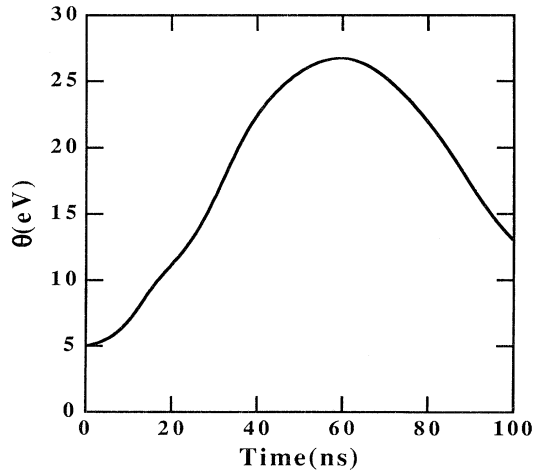

FIG. 6. The electron temperature Θ vs time for an optically thin Ne model of ion density 10^{18} cm^{-3}. The starting temperature 5 eV was chosen for convenience and does not affect the behavior near the peak of Na x-ray pulse at 52.5 ns.

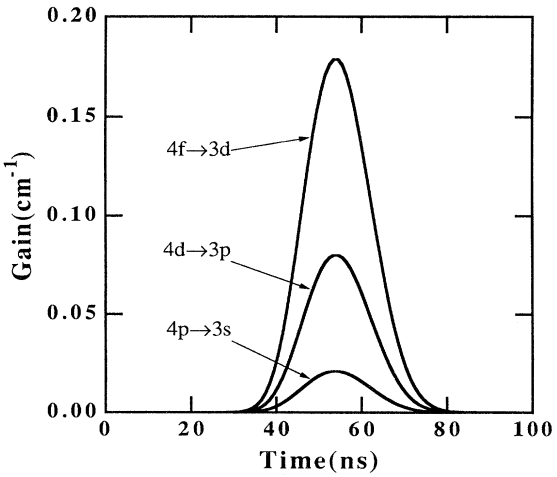

FIG. 8. Gain vs time for the three Ne $n=4\rightarrow3$ singlet laser lines in an optically thin model of ion density 10^{18} cm^{-3}. The largest gain is on the $4f\rightarrow3d$ transition at 231 Å.

strongest lines near 231 Å, $4f \rightarrow 3d$, $4d \rightarrow 3p$, and $4p \rightarrow 3s$. The peak gain of the strongest line $4f \rightarrow 3d$ is 0.179 cm^{-1} at 54 ns with a FWHM time duration of 18.5 ns. The gains of the two shorter wavelength lines, $3d \rightarrow 2p$ and $4d \rightarrow 2p$, are shown in Fig. 9. Both these lines are very weak with peak gains less than 0.025 cm^{-1}. These gains are summarized in Table I, which shows the values at peak x-ray illumination, 52.5 ns, for this optically thin case which is labeled 0 D. The actual peak of the gain occurs a few ns later, but is only a few percent larger in value.

These calculations are unrealistically optimistic because they are optically thin and do not include radiation transfer effects; realistic one-dimensional models which include the effects of optical thickness and radiation trapping will be described in the next section.

As mentioned earlier, all these calculations assume a fairly narrow linewidth of 0.78 eV, or 7.6 mÅ, for the Na He-α pump line. But what if the line were actually narrower or broader? Figure 10 plots the gain of the $4f \rightarrow 3d$ singlet line versus the linewidth of the Na He-α pump line at the time of peak x-ray illumination 52.5 ns. The total power in the Na He-α line is kept constant. As one would expect, the gain is proportional to the inverse of the linewidth. If the linewidth is doubled the gain is cut in half.

Let us try to understand the gain in the $4f \rightarrow 3d$ singlet laser line at 231 Å, from the relevant kinetic rates at the time of peak x-ray illumination, 52.5 ns. Recall that the Ne ion density is 1.0×10^{18} ions/cm^3 and the electron temperature is 26.1 eV. This results in an electron density of 7.56×10^{18} electrons/cm^3. The photon modal density n_ε of the pump line, in photons per mode, is calculated from the spectral intensity I_ε of the pump line, by

$$n_\varepsilon = \frac{(hc)^3}{8\pi c \varepsilon^3} I_\varepsilon = 1.579\times10^{-5}\frac{I_\varepsilon}{\varepsilon^3} , \quad (2)$$

where $\varepsilon = h\nu$ is the photon energy in eV, c is the speed of light, h is Planck's constant, and I_ε is the spectral intensity in $W/(cm^2\,eV)$. $I_\varepsilon \Delta\varepsilon$ is the power per unit area emitted into an energy bin of width $\Delta\varepsilon$. As a result, the Na He-α line has a pump strength of 5.65×10^{-5} photons per mode which leads to a stimulated photoexcitation rate of 0.147 ns^{-1} on the Ne He-γ line. The corresponding spontaneous emission rate for this transition is 866 ns^{-1}. If the only flux feeding the $4p$ state is due to photoexcitation from the ground state and there are no other significant decay mechanisms, then in the steady state the population of the $4p$ state N_{4p}, can be estimated by knowing the population of the He-like ground state, $N_{g.s.}$, and the strength of the He-like pump line n_ε using

$$N_{4p} = n_\varepsilon \frac{g_{4p}}{g_{g.s.}} N_{g.s.} , \quad (3)$$

where g_i is the degeneracy $(2J+1)$ of level i. Using $n_\varepsilon = 5.65\times10^{-5}$ photons per mode, and $N_{g.s.} = 5.26\times10^{17}$ cm^{-3} in Eq. (3) yields $N_{4p} = 8.92\times10^{13}$ cm^{-3}, which is three times larger than the value of 3.03×10^{13} cm^{-3} calculated by XRASER. This dilution of the population is due to collisional equilibration of the $4p$ level with the other $n = 4$ levels, which can then decay to other states. The resulting populations in the $4f$ upper laser state is 4.17×10^{13} cm^{-3}. The $4d$ upper laser state has a population of 3.85×10^{13} cm^{-3}. The collision rates from the $4p \rightarrow 4d$ and $4d \rightarrow 4f$ levels are 5270 and 1800 $nsec^{-1}$, respectively, with the reversed rates being in detailed balance. A disadvantage of this type of laser which relies on collisional transfer to populate the upper laser state is that many other states are populated which do not contribute to the gain.

If the lower laser state $3d$ is fed only by decay from the

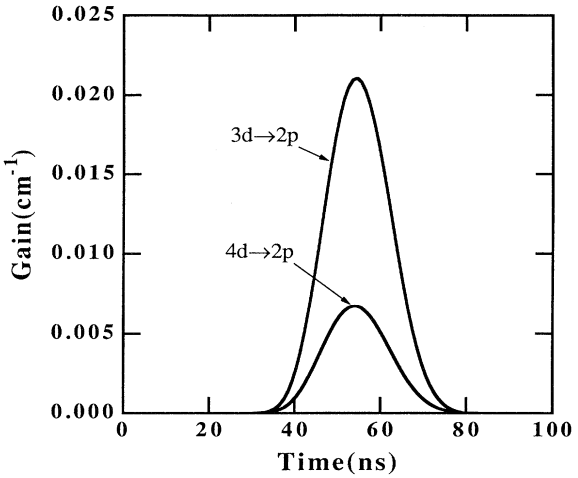

FIG. 9. Gain vs time for the two shorter wavelength Ne lasing lines with $2p$ lower lasing levels in an optically thin model of ion density 10^{18} cm^{-3}. These levels are susceptible to radiation trapping in realistic one-dimensional models, because the optically thick Ne He-α line increases the $2p$ population.

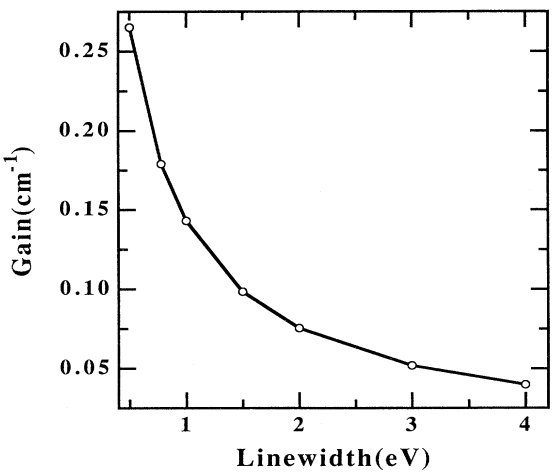

FIG. 10. Gain on the $4f \rightarrow 3d$ line vs linewidth of the Na He-α pump line at the time of peak illumination 52.5 ns, in an optically thin medium of ion density 10^{18} cm^{-3}. Our nominal calculations use the value of 0.78 eV; experiments show an instrument-limited linewidth of 4 eV.

$4f$ upper laser state, then its population N_{3d}, can be estimated as

$$N_{3d}=\frac{\gamma_{4f\rightarrow 3d}}{\gamma_{3d\rightarrow 2p}}N_{4f} \ . \tag{4}$$

The total rate from level i to j, γ_{ij}, is the sum of the collision rate γ^C and the radiative rate γ^R, which is also the spontaneous emission rate. For the $4f\rightarrow 3d$ transition, the collisional rate is 93.3 ns^{-1} while the radiative rate is 65.4 ns^{-1}. For the $3d\rightarrow 2p$ transition, the collisional rate is 40.1 ns^{-1} while the radiative rate is 388 ns^{-1}. Using these rates and the above-mentioned value of N_{4f} in Eq. (4) yields $N_{3d}=1.55\times 10^{13}$ cm^{-3}, which is 110% of the value of 1.39×10^{13} cm^{-3} calculated by XRASER, indicating that other mechanisms contribute slightly to the destruction rate of the $3d$ level.

The emission cross section σ for the $4f\rightarrow 3d$ gain line is given by

$$\sigma=\frac{\lambda^2}{2\pi}\frac{\gamma^R_{4f\rightarrow 3d}}{2\pi\Delta\nu_L}\sqrt{\pi}aH(a,x) \ , \tag{5}$$

where the Voigt parameter a and detuning x are given by

$$a=\frac{\Delta\nu_L}{2\Delta\nu_D} \ , \quad x=\frac{\nu-\nu_0}{\Delta\nu_D} \ ; \tag{6}$$

here $h\nu_0$ is the line center photon energy, $\Delta\nu_L$ is the FWHM Lorentzian linewidth, $\Delta\nu_D$ is the $1/e$ Gaussian half-width, and $H(a,x)$ is the Voigt function [28]. The small signal gain g_0 is calculated by

$$g_0=\left[N_{4f}-\frac{g_{4f}}{g_{3d}}N_{3d}\right]\sigma \ . \tag{7}$$

Using $a=0.353$, $x=0$, $2\pi\Delta\nu_L=3020$ ns^{-1}, and $H(a,x)=0.700$ in Eq. (5) yields a stimulated emission cross section $\sigma=8.06\times 10^{-15}$ cm^2. The result from Eq. (5) in Eq. (7) together with the populations calculated by XRASER gives a gain of 0.179 cm^{-1}, which is almost exactly what is calculated by XRASER.

It should be mentioned that the atomic model for Ne uses rates which have been calculated theoretically. Obviously, other atomic physics codes, or experiments, may yield different results for these rates. One very important rate is the spontaneous emission rate for the He-γ line. Other calculations [24] use a value of 1100 ns^{-1}, which is 27% larger than used in this paper, however when this change is incorporated in our model, the peak gain increases only by 15% to 0.205 cm^{-1}. Another uncertainty is the possible effect of ion-ion collisions in equilibrating the populations of the $n=4$ sublevels of Ne IX. To address this, as well as uncertainty in the electron-ion collision rates, we increased the $4d\rightarrow 4f$ collision rate mentioned previously by 50% to 2700^{-1}. This change results in only a 0.5% increase in the peak gain to 0.180 cm^{-1}. In our calculations the peak He-like Ne ground-state fraction is 53% while calculations [24] by Apruzese have yielded 80% in the He-like ground state. The higher He-like fraction would increase the gain by 50%. In calculating the Voigt linewidth for the laser line we do not include the effect of Dicke narrowing [29-32] which could increase the gain by 10% for the temperatures and densities used in this paper. Likewise, though the result is insensitive to the blackbody temperature, no measurement of the spectral shape of the low-energy x rays in the Na spectrum has been undertaken, adding to the uncertainty. An important point to keep in mind is that this is a difficult calculation with a fair amount of uncertainty.

How can we increase or better utilize the modest gain which is calculated? The gain can be increased by moving the Ne plasma closer to the Na Z pinch. It has been estimated [24] that moving the Na to 1.4 cm from the Na Z pinch will double the incident x-ray flux. In addition, recent shots at the Saturn facility have seen as much as 300 GW of power from the Na He-α line. If we combine these two effects the peak gain calculated is 0.518 cm^{-1}. In addition, there is a triplet line, $1s4f\,^3F_3\rightarrow 1s3d\,^1D_2$ with a peak gain of 0.075 cm^{-1} which is calculated to have a wavelength of 231.17 Å, in almost exact resonance with the singlet $4f\rightarrow 3d$ line calculated at 231.14 Å. If the gain of these two lines can be added, this increases the peak gain to 0.592 cm^{-1}.

To utilize these modest gains, an x-ray cavity could be built around this laser as was done for the Be-like C laser at 2163 Å. That 2163-Å laser had a single pass gain length product of 0.5, very similar to the Na-Ne laser. Placing the Be-like C gain medium in a Fabry-Pérot resonator enabled the experiments to achieve a net gain-length product of 4.5 after about 50 passes, resulting in an amplification of the spontaneous emission by two orders of magnitude. A similar procedure could be tried for the Na-Ne laser.

V. RADIATION TRANSFER

In this section we address the question of what happens to a finite-size region of Ne plasma with transverse dimensions of 0.6 cm. The calculations described in the preceding section indicate that the Ne He-γ resonance line being pumped has a peak absorption coefficient of 25 cm^{-1}, indicating that a 400-μm-thick laser would be approximately one mean free path thick to the pump radiation. However, radiation trapping of the Ne He-α line, which has a peak absorption coefficient of 480 cm^{-1}, enhances the population of the $2p$ level and thus lowers the gain on the $4d\rightarrow 2p$ and $3d\rightarrow 2p$ transitions; thus a plasma thicker than 20 μm will be optically thick to this radiation and probably will not support lasing on those transitions.

To model the finite-size system we did calculations in a one-dimensional (1D) slab geometry which assumes that the radiation from the Na Z pinch is incident normal to the surface of the slab starting at position $x=0$. For the Ne plasma we included radiation transfer calculations on the continuum radiation as well as 12 lines: the two Ly-α, two Ly-β, and two Ly-γ of H-like Ne and the He-α, He-β, He-γ, and the three corresponding intercombination lines for He-like Ne.

The Ne plasma is optically thin to the continuum x-ray radiation so the temperature is fairly isothermal across the 1D slab. The general ionization conditions described

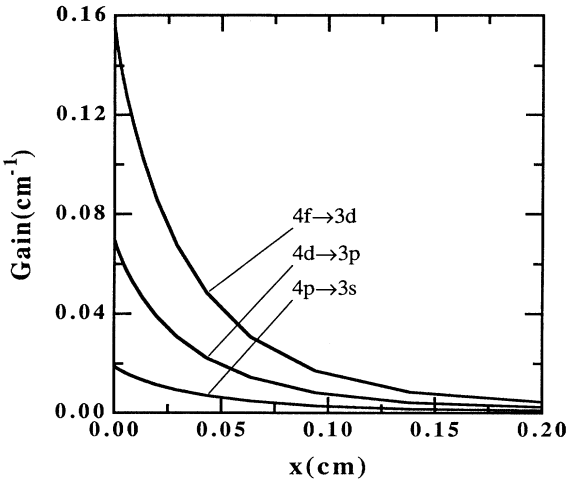

FIG. 11. Gain vs position x at the time of peak illumination, 52.5 ns, in a 0.6-cm thick Ne slab of ion density 10^{18} cm^{-3} for the three Ne $n=4\rightarrow3$ singlet laser lines in a 1D slab calculation which includes radiation transfer. The gain in these lines falls to half the maximum value within 250 μm of the surface.

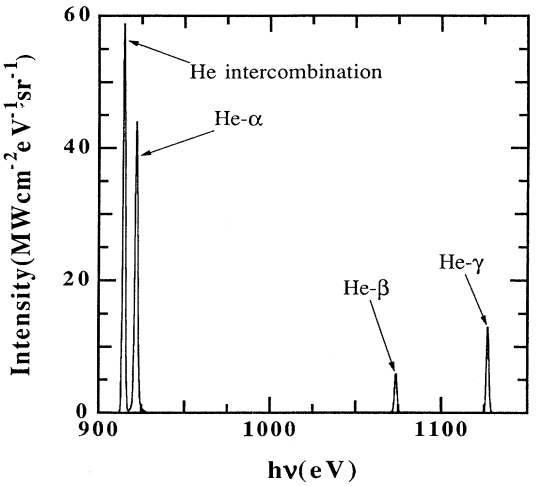

FIG. 13. The intensity of the He-α, He-β, and He-γ lines at the time of peak illumination, 52.5 ns, in a 0.6-cm thick Ne slab of ion density 10^{18} cm^{-3} as seen by an observer at 60° to the normal from the surface at position $x=0$. The lines calculated by XRASER have been convoluted with a Gaussian profile with a 1-eV $1/e$ half-width to approximate the source broadening and instrument resolution present in the Saturn experiments. The ratio of the He-γ to He-β intensities is approximately 2.2 to 1.

in the preceding section are representative of the Ne plasma anywhere in the slab. The major differences are that now the Na He-α line is being absorbed in a surface layer. The gain of the $4f\rightarrow3d$ line versus position across the slab at the time of peak x-ray illumination, shown in Fig. 11, peaks at $x=0.0$ cm with a value of 0.157 cm^{-1} and decreases to half this value at $x=0.024$ cm. Also shown are the other two lines near 231 Å which are weaker but have a similar falloff. If we now consider the shorter wavelength lines, Fig. 12 plots gain versus position across the slab at the time of peak x-ray illumination. Unlike the optically thin case presented in the preceding section, the gain is negative because the radiation trapping of the Ne He-α line feeds the lower laser state and destroys any inversion. These lines are actually weakly absorbing. The gains at the front surface of the 1D slab calculation are summarized in Table I, which shows the values at the time of peak x-ray illumination 52.5 ns.

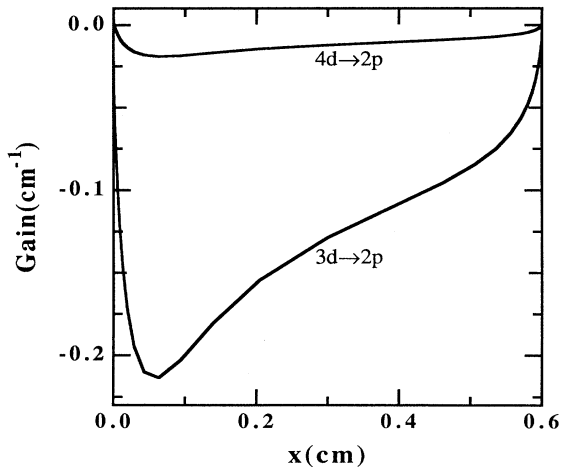

FIG. 12. Gain vs position x at the time of peak illumination, 52.5 ns, in a 0.6-cm thick Ne slab of ion density 10^{18} cm^{-3} for the two shorter wavelength Ne lines with $2p$ lower lasing levels in a 1D slab calculation which includes radiation transfer. The gain is destroyed because the opacity of the Ne He-α line causes population enhancement of the $2p$ level.

The quantity presently studied in experiments is the ratio of the He-γ to the He-β line. The assumption has been that an increase in this ratio for a Ne plasma pumped by a Na plasma as compared with the usual ratio for these line when there is no resonant line pumping the Ne plasma is an indication of gain in the system. Our calculations do support this hypothesis that a large ratio for the two lines implies a similar ratio for the $n=4$ to 3 population; that condition does not imply a large gain, however, since the absolute values of the populations in the $n=4$ and 3 levels may be quite small. Figure 13 plots the angle-dependent spectral intensity of the He-like lines viewed by an observer looking at 60° to the normal with the front surface of the Ne plasma which is illuminated by the Na Z pinch versus photon energy $h\nu$. The lines calculated by XRASER have been convoluted with a Gaussian profile with a 1-eV $1/e$ half-width to approximate the source broadening and instrument resolution present in the Saturn experiments. Under these conditions the ratio is 2.2 to 1 for the He-γ to He-β lines. This is very similar to the results seen in the recent Saturn experiments.

VI. CONCLUSIONS

This paper has presented an analysis of the Na-Ne x-ray-laser scheme under the conditions that have been

tried in recent experiments on the Saturn facility. The output of the Na Z pinch as measured at the Saturn generator has been used as the external x-ray source to illuminate a Ne plasma. The time-dependent plasma properties of that Ne plasma have been presented. The $4f \rightarrow 3d$ laser line at 231 Å, which is the strongest laser line, has a maximum gain of only 0.179 cm^{-1} in the calculations presented here; such a gain would be difficult to observe experimentally. We find that the gain persists for a long time, with a 18.5-ns FWHM pulse width. The gain may be increased by as much as a factor of 3 by moving the Ne plasma closer to the axis of the Na Z pinch. Alternatively, the long-time duration of the lasing suggests that an x-ray cavity could be built around the Ne plasma to increase its output. The shorter wavelength lines, $3d \rightarrow 2p$ and $4d \rightarrow 2p$, at 60 and 82 Å are calculated to have no gain and actually be weakly absorbing when the effects of radiation trapping are included in the calculations.

ACKNOWLEDGMENTS

The authors would like to thank Keith Matzen, John Porter, Rick Spielman, Gene McGuire, and Tom Hussey of Sandia National Laboratories for providing valuable information about the Saturn facility and the output characteristics of the Na Z pinch. John Apruzese from the Naval Research Laboratory provided important information concerning the modeling that had been done in the past for the Na-Ne scheme. K. T. Cheng and M. Chen of Lawrence Livermore National Laboratory graciously provided atomic models of Na and Ne for this work. An Institutional Research and Development grant from Lawrence Livermore National Laboratory supported part of this work. This work performed under the auspices of the U. S. Department of Energy by the Lawrence Livermore National Laboratory under Contract No. W-7405-ENG-48.

[1] A. V. Vinogradov, I. I. Sobel'man, and E. A. Yukov, Kvantovaya Elektron. (Moscow) **2**, 105 (1975) [Sov. J. Quantum Electron. **5**, 59 (1975)].
[2] B. A. Norton and N. J. Peacock, J. Phys. B **8**, 989 (1975).
[3] V. A. Bhagavatula, J. Appl. Phys. **47**, 4535 (1976).
[4] W. E. Alley, G. Chapline, P. Kunasz, and J. C. Weisheit, J. Quantum. Spectrosc. Radiat. Transfer **27**, 257 (1982).
[5] R. C. Elton, T. N. Lee, and W. A. Molander, Phys. Rev. A **33**, 2817 (1986).
[6] J. P. Apruzese, J. Davis, and K. G. Whitney, J. Appl. Phys. **53**, 4020 (1982).
[7] J. P. Apruzese and J. Davis, Phys. Rev. A **31**, 2976 (1985).
[8] J. P. Apruzese, G. Mehlman, J. Davis, J. E. Rogerson, V. E. Scherrer, S. J. Stephanakis, P. F. Ottinger, and F. C. Young, Phys. Rev. A **35**, 4896 (1987).
[9] F. C. Young, S. J. Stephanakis, V. E. Scherrer, B. L. Welch, G. Mehlman, P. G. Burkhalter, and J. P. Apruzese, Appl. Phys. Lett. **50**, 1053 (1987).
[10] S. J. Stephanakis, J. P. Apruzese, P. G. Burkhalter, G. Cooperstein, J. Davis, D. D. Hinshelwood, G. Mehlman, D. Mosher, P. F. Ottinger, V. E. Scherrer, J. W. Thornhill, B. L. Welch, and F. C. Young, IEEE Trans. Plasma Sci. **16**, 472 (1988).
[11] P. Monier, C. Chenais-Popovics, J. P. Geindre, and J. C. Gauthier, Phys. Rev. A **38**, 2508 (1988).
[12] J. Nilsen, Opt. Commun. **72**, 371 (1989).
[13] J. Nilsen, Phys. Rev. A **40**, 5440 (1989).
[14] B. N. Chichkov and E. E. Fill, Opt. Commun. **74**, 202 (1989).
[15] J. Nilsen, Opt. Commun. **78**, 51 (1990).
[16] J. Nilsen, Opt. Lett. **15**, 798 (1990).
[17] B. N. Chichkov and E. E. Fill, Phys. Rev. A **42**, 599 (1990).
[18] Y. T. Lee, W. M. Howard, and J. K. Nash, J. Quant. Spectrosc. Radiat. Transfer **43**, 335 (1990).
[19] J. Nilsen, Phys. Rev. Lett. **66**, 305 (1991).
[20] J. Nilsen, Phys. Scr. **43**, 596 (1991).
[21] T. Boehly, M. Russotto, R S. Craxton, R. Epstein, B. Yaakobi, L. B. Da Silva, J. Nilsen, E. A. Chandler, D. J. Fields, B. J. MacGowan, D. L. Matthews, J. H. Scofield, and G. Shimkaveg, Phys. Rev. A **42**, 6962 (1990).
[22] N. Qi and M. Krishnan, Phys. Rev. Lett. **59**, 2051 (1987).
[23] M. K. Matzen and J. L. Porter (private communications).
[24] John P. Apruzese (private communication).
[25] R. L. Kelly, J. Phys. Chem. Ref. Data. **16**, Suppl. 1, 186 (1987).
[26] P. L. Hagelstein and R. K. Jung, At. Data Nucl. Data Tables **37**, 121 (1987).
[27] J. Nilsen, in *Atomic Processes in Plasmas,* Proceedings of a Conference on Atomic Processes in Plasmas, Santa Fe, New Mexico, AIP Conf. Proc. No. 168, edited by Allen Hauer and A. L. Merts (AIP, New York, 1988), pp. 51–58.
[28] G. D. Finn and D. Mugglestone, Mon. Not. R. Astron. Soc. **129**, 221 (1965).
[29] R. H. Dicke, Phys. Rev. **89**, 472 (1953).
[30] D. D. Burgess, D. Everett, and R. W. Lee, J. Phys. B **12**, L755 (1979).
[31] S. G. Rautian and I. I. Sobel'man, Usp. Fiz. Nauk **90**, 209 (1967) [Sov. Phys.—Usp. **9**, 701 (1967)].
[32] H. R. Griem, Phys. Rev. A **33**, 3580 (1986).